ELSEVIER

Journal of Nuclear Materials 276 (2000) 251–257

journal of nuclear materials

www.elsevier.nl/locate/jnucmat

Quantitative analysis of CTEM images of small dislocation loops in Al and stacking fault tetrahedra in Cu generated by molecular dynamics simulation

R. Schäublin[a,*], A. Almazouzi[a], Y. Dai[b], Yu.N. Osetsky[c], M. Victoria[a]

[a] *Fusion Technology, Materials Group, CRPP, EPFL, EURATOM-Association-Swiss Conference, 5232 Villigen PSI, Switzerland*
[b] *Paul Scherrer Institute, 5232, Villigen PSI, Switzerland*
[c] *Materials Science and Engineering, Department of Engineering, The University of Liverpool, Liverpool L69 3BX, UK*

Abstract

The visibility of conventional transmission electron microscopy (CTEM) images of small crystalline defects generated by molecular dynamics (MD) simulation is investigated. Faulted interstitial dislocation loops in Al smaller than 2 nm in diameter and stacking fault tetrahedra (SFT) in Cu smaller than 4 nm in side are assessed. A recent approach allowing to simulate the CTEM images of computer generated samples described by their atomic positions is applied to obtain bright field and weak beam images. For the dislocation loop-like cluster it appears that the simulated image is comparable to experimental images. The contrast of the **g**(3.1**g**) near weak beam image decreases with decreasing size of the cluster but is still 20% of the background intensity for a 2 interstitial cluster. This indicates a visibility at the limit of the experimental background noise. In addition, the cluster image size, which is here always larger than the real size, saturates at about 1 nm when the cluster real size decreases below 1 nm, which corresponds to a cluster of 8 interstitials. For the SFT in Cu the **g**(6.1**g**) weak beam image is comparable to experimental images. It appears that the image size is larger than the real size by 20%. A large loss of the contrast features that allows to identify an SFT is observed on the image of the smallest SFT (21 vacancies).

1. Introduction

Irradiation of metals with energetic particles leads to displacement cascades that drive the formation of structural defects in the form of defect clusters that can be directly observed in transmission electron microscopy (TEM). Irradiation of metals with high energy heavy ions, protons or fast neutrons produces intra-cascade clusters in addition to Frenkel pairs, that can also be produced by electron irradiation. Such defect clusters are of great technological relevance as they may be stable up to high temperatures and are in general detrimental to mechanical properties.

Direct observation of the induced defect distribution and evolution is difficult because of the nanometric sizes of the early clusters and to the short times (less than a nanosecond) of the evolution of their nascent cascade [1]. In order to study the formation of defects from the early stages of the displacement cascade, molecular dynamics (MD) appears in this context an appropriate technique [2]. Defect clusters derived from MD simulations are however lacking direct TEM experimental confirmation because of the non-trivial relation between the defect cluster and its TEM image. More to the point, it is the defect size and type that are questioned here. On the experimental side there is a general agreement on the type of defect clusters that can be found in post-irradiation microstructural TEM examination when sizes are larger than about 2 nm. In face centered cubic metals, beside SFTs and voids originating from vacancy clusters, small clusters are in the form of faulted loops (Frank loops) that have a Burger's vector **b** equal to $a_0/3\langle 111\rangle$, where a_0 is the lattice parameter, and can be either vacancy or interstitial in nature [3–6]. The weak beam technique [7] seems the most appropriate in the

* Corresponding author. Tel.: +41-56 310 4082; fax: +41-56 310 4529.
E-mail address: robin.schaublin@psi.ch (R. Schäublin)

0022-3115/00/$ - see front matter
PII: S0022-3115(99)00219-6

case of small defects as it provides an improved spatial resolution and signal to background ratio over the usual bright/dark field mode of imaging in TEM.

The goal of this work is to investigate the correlation between the defect clusters generated by MD and their observation in TEM by simulating the conventional transmission electron microscopy (CTEM) images of pre-defined defect clusters using a novel technique. The present study focuses on interstitial Frank loops in Al and SFTs in Cu that are smaller than about 3 nm. Of particular interest are: (i) the visibility of the defect cluster in terms of image contrast, (ii) the limits to which its type can be identified by its TEM image features and (iii) the correlation between its real size and its TEM image size. We show here that this virtual microscopy allows not only to address the abovementioned points, but also to assess experimental TEM limitations for small defect clusters.

2. MD simulation method

Molecular dynamic simulations of the relaxation of interstitial Frank loop configurations in Al are achieved using MDCASK code [8] which is based on the embedded-atom method [9] and the link cell method that allows a fast neighbor search and a full parallelization. Calculation time is about 2×10^{-5} s/step/atom when using the PVM library on the Cray T3D and 5×10^{-6} s/step/atom when using the MPI library on the Silicon Graphics 0rigin 2000 of the Ecole Polytechnique Fédérale de Lausanne. The interatomic potential for Al used in this investigation is the one developed by Ercolessi and Adams [10] that is based on a fit to an ab initio calculation of the atomic forces of a many-atom configuration. This potential has a cut-off distance between the fourth and the fifth neighbor. Atomic configuration of the interstitial clusters are found by choosing a starting configuration roughly approximating the situation under consideration in the central region of a cubic box that contains 426 000 atoms. All the simulations have been performed using the constant volume and periodic boundary condition. Cluster size ranges from 2 to 37 $\langle 1\,1\,1\rangle$ dumbbells that are arranged on the (1 1 1) plane in such a way that the shape of the cluster is close to a disk. The actual shape for the larger loops is hexagonal with sides along $\langle 1\,1\,0\rangle$ directions. The relaxation procedure, that is described in more detail elsewhere [11], consists in decreasing dynamically the temperature of the system to 0 K. A final temperature of 10^{-5} K is reached by setting the velocities of the atoms equal to zero each time the velocity and acceleration vectors have opposite directions. The resulting configuration is believed to be fully relaxed.

Molecular dynamic simulation of the SFT configurations in Cu are achieved using a long-range pair interatomic potential [12] derived within the pair approximation of the generalized pseudopotential theory [13]. SFTs are created by removing a number of atoms in the central part of the spherical sample containing about 730 000 atoms. The resulting vacancies are on a (1 1 1) plane and form a triangle with sides along $\langle 1\,1\,0\rangle$ directions. In order to collapse the triangle of vacancies into the desired SFT a combination of conjugate gradient and quasi-dynamical relaxation is applied. The conjugate gradient method allows to reach a local minimum of energy by allowing atoms to descend their local potential energy slopes while the quasi-dynamical relaxation is obtained by a dynamical calculation of the atomic positions tempered by a damping of their kinetic energy. The combined approach allowed the defect configuration to reach an energy state lower than the state that is obtained by using solely a conjugate gradient relaxation. This relaxed configuration is believed to be the actual one. SFT sizes selected for this study are aimed at a range from about 1 to 3 nm. It should be noted that the perfectly triangular shape of the original cluster forces the number of vacancies to a limited set [14]. With this in mind, the original triangle is chosen to be formed with 21, 45 and 91 vacancies, which result in SFTs that have a side of 1.5, 2.3 and 3.3 nm, respectively. The change in size from a triangle to the next larger one corresponds here to the addition of 3 rows of vacancies on a side.

The resulting relaxed structures are then examined in the virtual TEM. It should be noted at this point that the number of atoms contained in the sample is unusually large when considering that for the cluster sizes considered here much smaller samples would have been sufficient to reasonably contain the full relaxation of the cluster and its surroundings. The goal of a large number of atoms is to allow for samples that have a thickness that can be compared with experimental TEM sample thickness. Ideally for CTEM and more precisely for weak beam the sample should be more than 10 nm thick to avoid surface effects and thinner than 80 nm [15] to reduce anomalous absorption, which arises from inelastic scattering of the electrons, that will blur the image.

3. CTEM simulation method

The CTEM images of the defect clusters are simulated using the multislice method [16] to obtain their weak beam image at 200 kV. The imaging conditions have an influence on the quantification of the actual defect from its image. On the imaging side the parameters of importance are the objective aperture size, the

spherical aberration, the beam convergence, and the defocus spread. Regarding the sample itself, its thickness and the depth of the defect cluster are the main parameters. The latter parameters can be changed and the resolution limit that could be ideally achieved can be so explored. Indeed, limitations are imposed experimentally by sample preparation quality and unwanted structural defects. The technique used here is derived from the multislice technique that was originally developed to simulate high resolution TEM images. A number of approximations described in the next paragraph are applied in order to simulate the CTEM images.

The CTEM image simulation is performed here with the EMS software [17] that includes the multislice technique. Only the main elements of the approach are given here as more details on the way the multislice technique can be used to simulate CTEM images are given elsewhere [18]. Basically, the sample derived from the MD simulations is cut perpendicular to the electron beam direction in slices 0.2 nm thick. The sampling in all cases is chosen to be 1024×1024 for slices that are roughly 10 nm in side and contain roughly 2000 atoms. The diffraction condition is selected by the beam direction, which is also the cutting direction, so that it allows isolating the systematic row defined by the selected diffraction vector. Slices have to be periodic because the multislice method is based on Fourier transforms. In order to comply with this rule the cut direction is chosen to be a crystallographic direction that is close to the originally desired direction. For CTEM imaging a single systematic row should be operating. The use of a crystallographic direction for the cut introduces secondary families of diffracting planes that may disturb the image. In order to reduce the amount of the contribution of these secondary systematic rows, relatively high order crystallographic directions are chosen. It should be noted that one of the advantages in the use of the multislice approach over the classical beam calculation used for defects defined by their displacement field described by the elasticity of the continuum (see for instance [19]) is that it allows one to avoid the deformable ion approximation [20] which may be detrimental for defects as small as the ones that are considered here. In addition, this technique allows avoiding the column approximation generally used in the beam calculation. The parameters used to derive the images are close to those of modern microscopes which usually are operated at an acceleration voltage of 200 kV. For the present CTEM image simulations the beam semi-convergence, the defocus spread and the spherical aberration are set to zero in order to avoid extraneous effects from parameters that are generally not controlled in this imaging mode. In addition, absorption (both normal and anomalous) is not considered here. Table 1 gives the parameters used for the CTEM image simulations.

Table 1
CTEM image simulation parameters for the interstitial loop-like clusters in Al and the SFTs in Cu

	Loop in Al	SFT in Cu
Sample normal	[0 1 5]	[−3 2 0]
g vector	(2 0 0)	(0 0 2)
Slice dimension (nm^2)	11.7×11.3	14.5×14.4
Sample thickness (nm)	12.0	13.6
Diffraction condition	**g**(3.1**g**)	**g**(6.1**g**)
Deviation error (nm^{-1})	0.065	0.196
Effective extinction distance (nm)	15.1	5.1

4. Results and discussion

4.1. Interstitial loop-like clusters in Al

In the following, the definition of the loop size is given before proceeding to the CTEM image simulation results. Interstitial loops on the (1 1 1) plane in Al are defined by placing a number of atoms between two (1 1 1) planes to form a platelet as circular as possible. However, when exploring sizes smaller than 2 nm, the dimension is such that the cluster cannot be defined anymore as a loop. Nonetheless, in the following the loop is characterized as a loop-like cluster. This allows defining sizes down to 2 interstitials as the equivalent diameter of a disk that encloses the cluster. Disk surface is given by the number of interstitials in the cluster multiplied by the area occupied by one atom on a {1 1 1} plane. This area is given by $(\sqrt{3}/4)a_0$. Fig. 1 shows the resulting correlation between the real size and the number of SIAs in the cluster.

Fig. 2 shows a view along [−1 1 0] of the interstitial dislocation loop on (1 1 1) in Al for three different

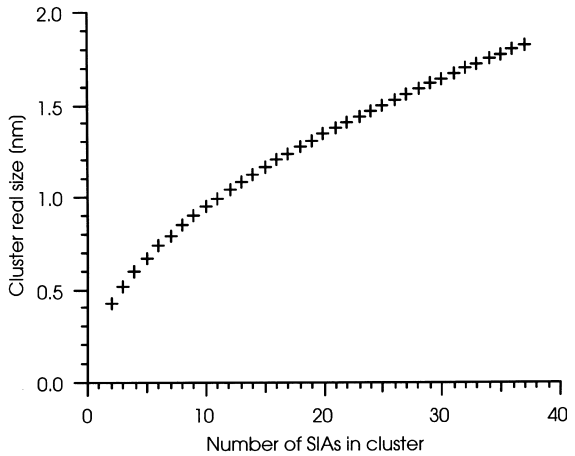

Fig. 1. Real loop-like cluster size in Al as a function of its number of self-interstitial atoms. It is the equivalent diameter of the disk that encloses the cluster that is constructed to tend to a circular loop on the (1 1 1) plane.

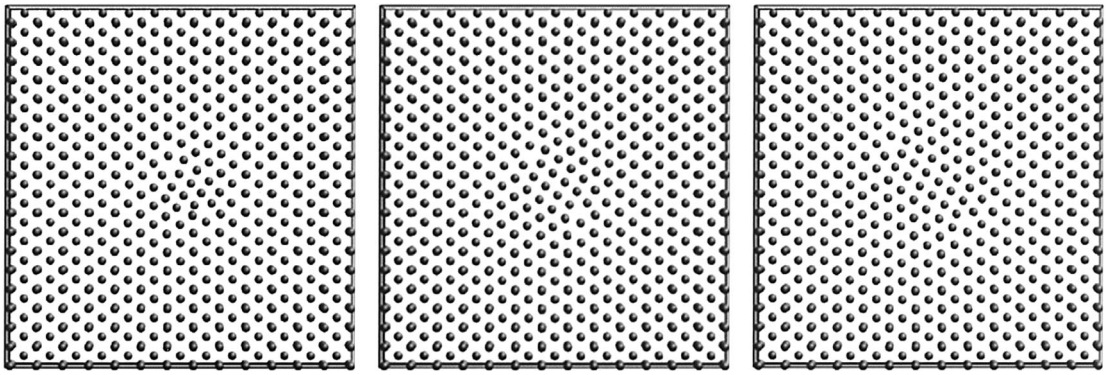

Fig. 2. View along [−1 1 0]of an interstitial dislocation loop on (1 1 1) in Al for a diameter of about (left) 1.0 nm (8 interstitials), (middle) 1.5 nm (19 interstitials) and (right) 2.0 nm (37 interstitials).

diameters. The 2 and 1.5 nm loops exhibit clearly the extra atomic plane bounded by the core of the dislocation loop, which has a Burgers vector **b** of $a_0/3[1\,1\,1]$. In the case of the 1 nm loop the extra plane, though distorted, is still discernable. The **g**(3.1**g**) near weak beam simulated images of these loops shown in Fig. 3 exhibit black and white lobes that are characteristic for inclusions in dynamical imaging conditions [21]. It should be noted that the present condition **g**(3.1**g**) does not fulfill the ideal weak beam conditions, one of which is that the deviation parameter is 0.2 nm^{-1} or larger [22]. The present deviation parameter is 0.065 nm^{-1} (see Table 1). This is the reason why the present condition is termed near weak beam. Under a true weak beam condition the dislocation loop should look like a single black or white dot. However, it should be noted that the way the gray levels are scaled for the display gives rise to an artificial enhancement of the back and white lobe contrast. When the images are displayed with a background value of 0.0 and not the minimum of the image, the image exhibits a black lobe that is somewhat smaller than the white lobe. The way to display simulated images in the most appropriate way remains unclear.

For the present particular case of Frank loops the line **l** joining the black to the white lobe is parallel to the Burgers vector **b** [3]. It should be noted here that the gray range of the printed figure is scaled artificially in order to render all contrast features of the images visible. Interestingly it appears that while the image orientation (**l**) is stable for loops larger than 1.5 nm there is a rotation of the black and white lobe axis towards the horizontal of the image, which is the direction of the **g** vector, for smaller loops. It indicates that when the loop becomes smaller its displacement field resembles more that of a spherical inclusion. This fact could be exploited experimentally in order to identify the size range for loops smaller than 2 nm in diameter when the contrast conditions are not ideal, or in other words when the image background intensity noise level is unusually high, so that the resolution is degraded. However, it appears that a loop-type cluster having a size in this range will be difficult to distinguish from a 3-dimensional interstitial cluster with the same diameter as the latter also gives an Ashby Brown-type contrast. It should be noted that bright field simulated images in the same condition, i.e. **g**(3.1**g**), not reported here show a single and featureless dot.

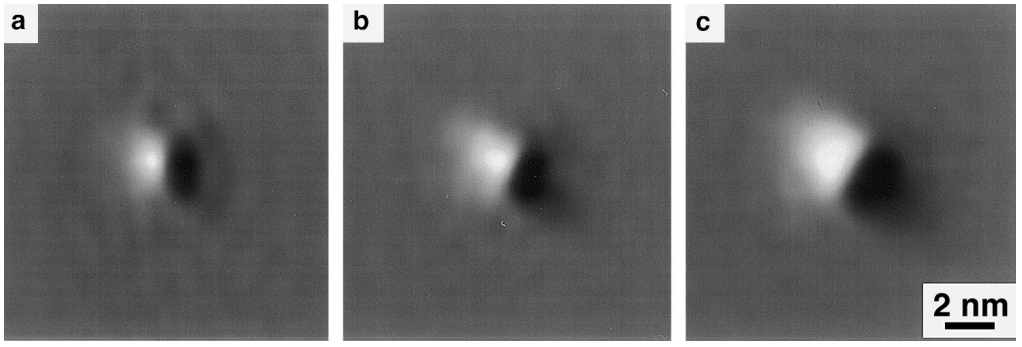

Fig. 3. Interstitial Frank loop-simulated TEM images using near weak beam **g**(3.1**g**), **g** = (2 0 0) at 200 kV in Al for a diameter of about (a) 1.0 nm (8 interstitials), (b) 1.5 nm (19 interstitials) and (c) 2.0 nm (37 interstitials).

Fig. 4 shows the contrast level of the **g**(3.1**g**) condition images as a function of the loop-like cluster real size. Relative contrast is defined as (Max – Back)/Back where Max is the maximum contrast level and Back is the background intensity level. It appears that, while there is a tendency to saturation for the minimum contrast level (Min) for sizes larger than 1.3 nm, the relative contrast does not present any trend for saturation for the sizes explored here. In addition, the relative contrast level starts from 20%, for the 2-interstitial cluster, and increases to 170% for the bigger loops. 20% intensity above background was indicated as an experimental value above which contrast can be differentiated from background on the printed media [3]. This indicates that the 2-interstitial cluster may be just visible in experimental conditions where background intensity noise level is commonly ±10% for metallic samples that are considered to be clean [18]. It should be noted that the bright field simulated images in the same condition, i.e. **g**(3.1**g**), have a contrast that is lower than the corresponding weak beam images. The weakness of this contrast indicates that this mode is not appropriate for the loop sizes considered here. The highest bright field contrast attained is 4% with the 37-interstitial cluster.

The size of the **g**(3.1**g**) near weak beam image of the loop-like cluster is measured with a ruler on the printed image which gray scale range is set constant for all cluster sizes. The gray scale range limits are chosen to be the extrema of the image intensity over all cluster sizes. This measurement procedure allows following the same technique applied experimentally with all the biases that it implies, such as the subjectivity of individuals. While the non-linear photographic response of the negative is not taken into account in the present study, and assuming that images are experimentally recorded using linear response media such as CCD cameras, the present results can be best compared with experimental results only when applying this procedure.

It appears as expected that the size of the image of the loop decreases with the real size. Fig. 5 shows the cluster image size as a function of the cluster real size. It appears that the image size is always larger that the real size. The enlargement might be expected when considering the fact that the observed contrast of a crystalline defect originates from the surrounding displacement field it induces, which is for the defect sizes considered here larger than the geometrical size of the defect. The width of a dislocation image for instance was estimated to be about one third of the effective extinction distance [7] for the considered diffraction condition. This rule of thumb however cannot be applied as such to three-dimensional defects. It appears that the image size saturates at about 1 nm when the loop-like cluster size reaches 1 nm and below. This saturation can be related to the fact that, in addition to the abovementioned relation to the extinction distance, the objective aperture cuts spatial frequencies. The limit in resolution is 0.7 nm for the 2.5 nm^{-1} aperture considered here. Experimentally however the specimen quality is one of the strongest limiting factors for resolution [6] and will further degrade the resolution. Nonetheless, weak beam technique has in many instances proved its improved resolution over bright and dark field imaging modes as for example in the resolution of partial dislocations in Ni_3Al separated by a little less than 1 nm [23]. It should be noted that image matching techniques have to be applied in these cases where quantitative information is desired.

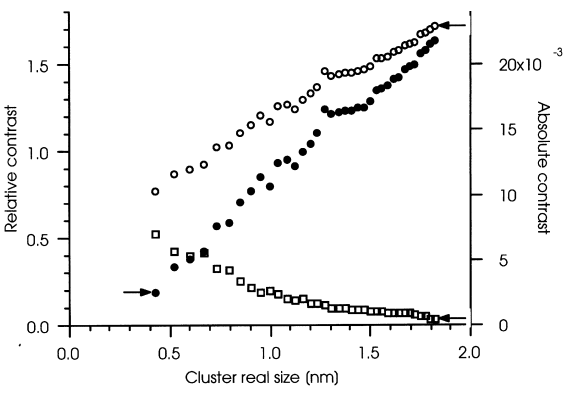

Fig. 4. Image contrast of the (1 1 1) loop-like cluster using near weak beam **g**(3.1**g**), **g** = (2 0 0) at 200 kV in Al as a function of its real size.

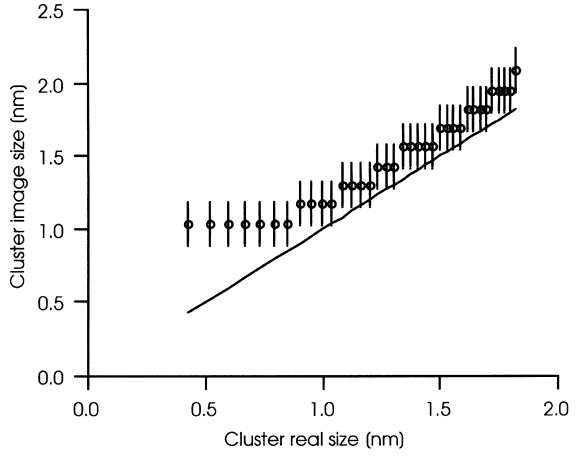

Fig. 5. Image size on the near weak beam **g**(3.1**g**), **g** = (2 0 0) at 200 kV in Al of the (1 1 1) loop-like cluster as a function of the real size.

4.2. Stacking fault tetrahedra in Cu

Experimental observations of SFTs in Cu were reported in [24]. The Cu single crystal has a purity of more than 99.99% with 1, 1 and 10 ppm of H, N and O, respectively. It was irradiated to 3.9×10^{-2} dpa at room temperature with 590 MeV protons and a dose rate of 1.8×10^{-7} dpa/s. Fig. 6 shows an experimental TEM weak beam $\mathbf{g}(6.1\mathbf{g})$, $\mathbf{g}=(0\,0\,2)$ image of the irradiated Cu sample. Defect clusters generated by the irradiation are mainly SFTs that appear as white and dark triangles. The size distribution peaks at about 2 nm.

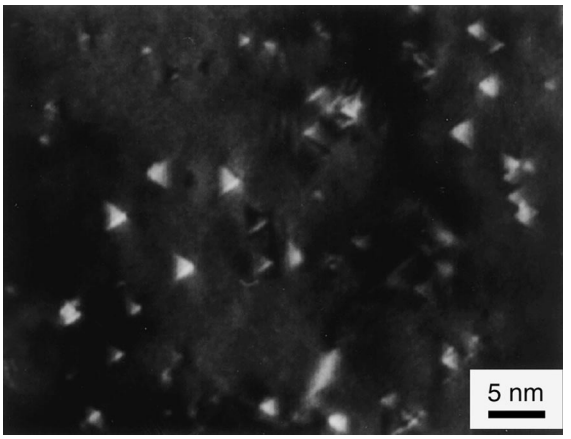

Fig. 6. Experimental TEM weak beam image $\mathbf{g}(6.1\mathbf{g})$, $\mathbf{g}=(0\,0\,2)$, in Cu irradiated with 590 MeV protons to a dose of 3.9×10^{-2} dpa. Defect clusters are mainly SFTs.

Fig. 7 shows SFT-simulated TEM images using weak beam $\mathbf{g}(6.1\mathbf{g})$, $\mathbf{g}=(0\,0\,2)$ at 200 kV in Cu as a function of SFT size and sample thickness. The side length of the SFT containing 21 vacancies (top image line) is 1.5 nm, that of the 45-vacancies SFT (middle image line) is 2.3 nm and that of the 91-vacancies SFT (bottom image line) is 3.3 nm.

The 91-vacancy SFT shows features that can be recognized in the experimental picture displayed in Fig. 6. Depending on the sample thickness, or alternatively on the cluster depth, the SFT appears as a white triangle or as a dark triangle. A close inspection of the image shows that the triangular image exhibits always a more intense side as on the experimental image, whether the triangle appears white or black. For the 45 vacancy SFT a detailed size analysis showed that the image size is 20% larger than the real size [25]. It appears that the difference is even larger when the triangle appears dark. When the SFT is 21 vacancies the image is actually smaller than the real size. This is due to the fact that the intensity contrast is much lower than in the case of the 45- or 91-vacancy clusters. When a bright field kinematical condition is considered, further simulations show that the SFT displays the same type of contrast as for the smallest size, that is to say a single featureless dot which is black. This mode was suggested to help in the measurement of the size of SFTs [6]. However, it should be noted that this contrast could be misinterpreted as the image of a dislocation loop or a 3-dimensional interstitial cluster in the same imaging conditions.

When compared to the dislocation loops, SFTs always exhibit a lower absolute contrast. This can be ex-

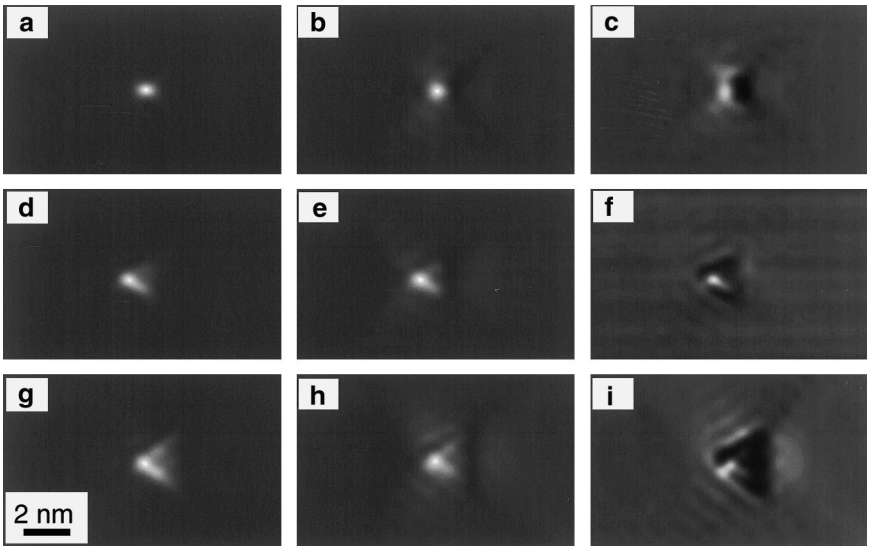

Fig. 7. SFT-simulated TEM images using weak beam $\mathbf{g}(6.1\mathbf{g})$, $\mathbf{g}=(2\,0\,0)$ at 200 kV in Cu as a function of SFT size and sample thickness. 21-vacancies SFT in a sample (a) 10.4 nm, (b) 11.6 nm and (c) 13.2 nm thick. 45-vacancies SFT in a sample (d) 13.6 nm, (e) 12.0 nm and (f) 15.2 nm thick. 91-vacancies SFT in a sample (g) 10.4 nm, (h) 11.6 nm and (i) 13.2 nm thick.

plained by the fact that the SFTs induce a displacement field in the surroundings that is smaller than the one induced by a Frank loop. Indeed, the stair-rod dislocations delimiting the SFT have a Burgers vector of $a_0/6\langle 1\,1\,0\rangle$ that is smaller in magnitude than the Burgers vector $a_0/3\langle 1\,1\,1\rangle$ of the dislocation delimiting the loop.

5. Conclusion

The results presented here show that this novel technique of image simulation might be used with confidence to close the gap between the MD simulations results and the experimental results deduced from TEM. For the dislocation loop-like cluster in Al simulated using molecular dynamics it appears that the simulated image is comparable to experimental images. On the **g**(3.1**g**) weak beam image the contrast which decreases with decreasing size is still 20% of the background intensity for a 2 interstitial cluster which indicates a visibility at the limit of the experimental background noise. In addition, the cluster image size, which is here always larger than the real size, saturates to about 1 nm when the cluster real size decreases below 1 nm, which corresponds to a cluster of 8 interstitials.

For the SFT in Cu the simulated **g**(6**g**) weak beam image obtained from MD samples is also comparable to experimental images. It appears that the image size is larger than the real size by 20%. A large loss of the contrast features that allows to identify an SFT is observed on the image of the smallest SFT (21 vacancies). This means that SFTs smaller than 21 vacancies will be difficult to identify on experimental CTEM images.

Acknowledgements

The Swiss National Fund for Science is acknowledged for financial support. Professor P. Stadelmann of the center of electron microscopy of the EPFL is gratefully acknowledged for his continuous help.

References

[1] R.S. Averback, D.N. Seidman, Mater. Sci. Forum 15–18 (1987) 963.
[2] D.J. Bacon, T. Diaz de la Rubia, J. Nucl. Mater. 216 (1994) 275.
[3] M. Rühle, in: Radiation Damage in Reactor Materials, International Atomic Energy Agency, vol. 1, 1969, p. 113.
[4] B.L. Eyre, J. Phys. F 3 (1973) 422.
[5] M. Kiritani, J. Nucl. Mater. 133–134 (1985) 85.
[6] M.L. Jenkins, J. Nucl. Mater. 216 (1994) 124.
[7] D.J.H. Cockayne, I.L.F. Ray, M.J. Whelan, Philos. Mag. A 20 (1969) 1265.
[8] T. Diaz de la Rubia, M.W. Guinan, J. Nucl. Mater. 174 (1990) 151.
[9] M. Daw, M.I. Baskes, Phys. Rev. B 29 (12) (1984) 6443.
[10] F. Ercolessi, J.B. Adams, Europhys. Lett. 26 (1994) 883.
[11] A. Almazouzi, B.D. Wirth, M. Alurralde, M. Victoria, Philos. Mag., to be submitted.
[12] Yu.N. Osetsky, A.G. Mikhin, A. Serra, Philos. Mag. A 72 (1995) 361.
[13] J.A. Moriarty, Phys. Rev. B 42 (1990) 1609.
[14] Y.N. Osetsky, M. Victoria, A. Serra, S.I. Golubov, V. Priego, J. Nucl. Mater. 251 (1997) 34.
[15] W.M. Stobbs, C.H. Sworn, Philos. Mag. 24 (1971) 1365.
[16] J.M. Cowley, A.F. Moodie, Acta Crystallogr. 10 (1957) 609.
[17] P.A. Stadelmann, Ultramicroscopy 21 (1987) 131.
[18] R. Schäublin, Philos. Mag. Lett., to be submitted.
[19] R. Schäublin, P. Stadelmann, Mater. Sci. Eng. A 164 (1993) 373.
[20] P.B. Hirsch, A. Howie, R.B. Nicholson, D.W. Pashley, M.J. Whelan, Electron Microscopy of Thin Crystals, Butterworths, London, 1969, p. 218.
[21] M.F. Ashby, L.M. Brown, Philos. Mag. 8 (1963) 1083.
[22] D.J.H. Cockayne, J. Microsc. 98 (2) (1973) 116.
[23] N. Baluc, R. Schäublin, Philos. Mag. A 74 (1) (1996) 113.
[24] Y. Dai, M. Victoria, Mater. Res. Soc. Symp. Proc. 439 (1997) 319.
[25] R. Schäublin, Y. Dai, M. Victoria, Electron Microscopy 1998, in: H.A. Calderón Benavides, M. J. Yacamán (Eds.), Proceedings of the 14th International Congress on Electron Microscopy, Cancun (Mexico), vol. I, Institute of Physics, Publishing, Bristol, 1998, p. 173.